A novel K-ion KVPO4F0.5O0.5/graphite full cell: Correlation between XPS SEI studies and electrochemical testing results

Badre Larhrib, Lénaïc Madec, Laure Monconduit, Hervé Martinez

A Novel K-ion $KVPO_4F_{0.5}O_{0.5}$/graphite full cell: Correlation between XPS SEI Studies and Electrochemical testing results

Badre Larhrib[a], Lénaïc Madec[a,c,*], Laure Monconduit[b,c], Hervé Martinez[a,c]

[a] Universite de Pau et des Pays de l'Adour, E2S UPPA, CNRS, IPREM, Pau, France

[b] ICGM, Université de Montpellier, CNRS, Montpellier (France)

[c] Réseau sur le Stockage Electrochimique de l'Energie, CNRS FR3459, Amiens, France

* Corresponding author: lenaic.madec@univ-pau.fr

ABSTRACT

Like Li- and Na-ion batteries, electrolyte reactivity (i.e., salt and solvent decomposition) is important in the electrochemical performance of K-ion batteries (KIBs). Indeed, X-ray photoelectron spectroscopy (XPS) analysis of a solid electrolyte interphase (SEI) in KIBs is still based on K-ion half-cells. This may lead to incorrect interpretations of the results considering the contamination of the studied electrode SEI due to the high K metal reactivity. Therefore, this study aims to provide a reliable XPS study without potassium metal, investigating the impact of various parameters, including open-circuit voltage (OCV) temperature, upper cut-off voltage (UCV), depth of discharge (DOD), and vanadium dissolution, on the electrochemical performance of $KVPO_4F_{0.5}O_{0.5}$/graphite full cells. This work highlights the importance of SEI preformation, which is more pronounced at higher OCV temperatures. At specific UCV and DOD, the cell provides the best trade-off between the organic and inorganic passivation layer, leading to good electrochemical performance. The study also demonstrates that vanadium dissolution is a potential mechanism affecting capacity fading in K-ion batteries. Finally, understanding these SEI growth mechanisms should help researchers get reliable XPS analysis of the SEI in KIBs and move forward with the practical passivation layer characterizations.

Keywords: $KVPO_4F_{0.5}O_{0.5}$//graphite K-ion cells, Upper cut-off voltage, Depth of discharge, SEI, XPS.

1. INTRODUCTION

The market for batteries includes numerous applications, from portable electronics, electric vehicles, grid storage etc. The demand for batteries will continue to grow as the use of electric vehicles and renewable energy sources increases **[1]**, so that alternatives to the Li-ion batteries are needed. In that direction, K-ion batteries (KIBs) present several advantages as a potential battery technology **[2]**. The most important ones are that potassium is much more abundant (2.1% by mass of the earth's crust and the sixth most abundant element dissolved in seawater) and inexpensive than lithium **[3]**. Moreover, the low standard redox potential of K^+/K (2.93 V versus the standard hydrogen electrode (SHE)), which is close to that of Li^+/Li (3.04 V versus SHE), implies possible high energy density. In addition, high power density is expected due to the lowest Lewis acidity and desolvation energy of K^+ compared to Na^+ and Li^+, *i.e.* the higher ionic conductivity and faster diffusion kinetics at the electrode/electrolyte interface, respectively. Also, inexpensive aluminum foil (instead of copper) can be used as negative electrode current collector. Finally, similarly to Li-ion batteries, and unlike Na-ion batteries, the reversible electrochemical intercalation of K ions into graphite has been experimentally demonstrated, making K-ion batteries as a potentially more sustainable and cost-effective alternative **[3,4]**.

However, some challenges need to be overcome to develop efficient KIBs. Beyond the active materials choice, the stability of active materials and electrolytes, including the electrode/electrode interfaces upon storage/cycling, are of high interest to understand KIBs failure mechanism and thus optimize KIBs lifetime **[5]**. To do so, the solid electrolyte interfase (SEI) formation and evolution upon storage/cycling as function of solvents/salts/additives needs to be urgently investigated/understood **[6–9]**. In that direction, some of us recently showed that the electrolyte reactivity at the K metal electrode governs half-cells performance and that more importantly that SEI cannot be study in half cells. Indeed, electrolyte degradation species formed at the K metal surface migrate to the working electrode and thus contaminate the studied electrodes whatever the electrolyte/electrode [9]. Thus, a reliable SEI study requires full-cells to prevent the K metal cross-contamination. However, while many papers have used X-ray photoelectron spectroscopy (XPS) to characterize the SEI layers in K-ion half-cells [7,10–18], to our knowledge, no studies have been performed so far to thoroughly investigate SEI in K-ion full cells **[5]**.

To address these issues, this work investigates the impact of OCV temperature, upper cut-off voltage, depth of discharge, and vanadium dissolution on the electrochemical performance

with a correlation to the SEI formation (analyzed by XPS) for $KVPO_4F_{0.5}O_{0.5}$//graphite full-cells. To do so, $KVPO_4F_{0.5}O_{0.5}$ was selected for its electrochemical performance **[19]** while optimized graphite electrodes [20] and optimized full-cells assembly (with highly reproducible and reliable results) were used [21].

2. EXPERIMENTAL

Materials and electrodes preparation

Graphite electrodes were prepared following a previously optimized formulation [20]: SLP30 (TIMCAL), Carbon black (CB, C65, MTI), Carboxymethyl Cellulose (CMC-Na, Sigma-Aldrich, Mw ~250000), and carboxylated Styrene Butadiene Rubber (SBR, LITEX LB-420, Synthomer) were mixed with an 85:5:8:2 weight ratio in 1 ml distilled water using ball milling (PULVERISETTE 7) at 500 rpm for 1h. The slurry was coated on aluminum foil (15 µm thickness) by a doctor blade (125 µm corresponding to 2.4 $mg_{graphite}$ cm^{-2}). Then the film was dried at room temperature for 1 night and 11 mm diameter electrodes were cut out, pressed at 2 tons / cm^2 (leading to ~35% electrode porosity), and dried again under vacuum at 80 °C for 12 h.

$KFPO_4F_{0.5}O_{0.5}$ (KVPFO) samples were synthesized by solid-state reaction previously reported [19]. Electrodes were prepared by mixing KVPFO, CB (C65, MTI), and Polyvinylidene fluoride (PVDF 5130, Solef) with a 75:15:10 weight ratio in 2.5 ml N-Methyl-2-pyrrolidone (2.5 mL NMP for 1g) using ball milling (PULVERISETTE 7) at 500 rpm for 1h. The slurry was coated on aluminum foil (15 µm thickness) by a doctor blade (300 µm corresponding to 5 mg_{KVPFO} cm^{-2}). The film was then dried at 60°C for 12h under air. Then, 9.5 mm diameter electrodes were cut out, pressed at 3 tons/cm^2 (leading to ~36% electrode porosity), and dried again under vacuum at 80 °C for 12 h.

Electrochemical testing

KVPFO//graphite cells were assembled using previously optimized cell parameters, *i.e.* with electrode diameter and capacity ratio fixed to 1.16 and an electrolyte volume of 50µL Electrochemical experiments were conducted using a VMP 3 multichannel system (BioLogic, France) in a 20°C temperature-controlled room. Two pairs of coin cells (CR2032, stainless steel 316L) were assembled for reproducibility, while in the results section, data for only one cell is presented for clarity. The electrolyte was 0.8 M KPF_6 (Sigma-Aldrich, 99%) EC:DEC

(ethylene carbonate, Sigma-Aldrich, 99%, and diethyl carbonate, Sigma-Aldrich, 99%) by volume. Two microporous trilayer membranes (PP/PE/PP, from Celgard) were used as separators.

Galvanostatic cycling was made in full coin-cells as follows:

First, the OCV before cycling was done at 25°C, 40°C or 60°C for 12 hours to investigate its impact on the pre-formation of SEI analyzed by XPS. Additional cells were then cycled 50 times at C/10 between 1.2-4.8 V.

Second, the impact of the upper cut-off voltage on the SEI was performed selecting the OCV at 40°C followed by 50 cycles at C/10 between 1.2-4.5 V, 1.2-4.8 V or 1.2-5.0 V.

Third, the impact of the lower cut-off voltage on the SEI was performed selecting the OCV at 40°C followed by 50 cycles at C/10 between 1.2-4.8 V, 2.0-4.8 V, and 3.0-4.8 V.

X-ray diffraction and Raman spectroscopy

The X-ray diffraction (XRD) data was collected using a PANalytical X'Pert Pro-MPD diffractometer that employed a copper Kα radiation source with a wavelength of 1.5418 Å and a step size of 0.033°, within a range of 10° to 40°. Furthermore, an ex-situ Raman spectrum was acquired using a Horiba Jobin-Yvon LabRAM ARAMIS spectrometer, operated with an excitation wavelength of 473 nm for the measurements.

Ex situ X-Ray photoelectron spectroscopy (XPS)

XPS characterization was performed using an Escalab 250 Xi spectrometer with a monochromatized Al Kα radiation (hν = 1486.6 eV). KVPFO and graphite electrodes, as obtained after the OCV at different temperatures or after 50 cycles as function of the upper and lower cut off voltages, were placed on a sample holder using uPVC insulation tape (3 M part number 655) and transferred to an argon-filled glove box connected to the spectrometer to avoid moisture/air exposure. Analysis was performed using the standard charge compensation mode and an elliptic 325 × 650 μm X-ray beam spot. Core level spectra were recorded using a 20 eV constant pass energy with a 0.15 eV step size and iterative scans with a dwell time of 500 ms to follow any possible degradation. Using CasaXPS software, the binding energy scale was calibrated from C-C, C-H peak at 285 eV. A non-linear Shirley-type background was used for core peaks analysis while 70% Gaussian - 30% Lorentzian Voigt peak shapes (called GL(30)), full width at half-maximum, and position constraint ranges were

selected to optimize peak positions and areas. Peak attribution was based on previous studies [12,22], including a K reference compound database previously reported by some of us [23].

For more clarity, the SEI composition resulting from XPS quantification (**Tables S1 and S2**) of graphite and KVPFO electrodes will be illustrated in a 3D pie chart.

Graphite and KVPFO electrodes were rinsed 2 times during 1 min in 2 ml of pure DEC (anhydrous, >99% purity, Aldrich) and dried inside the argon-filled glove box for 5h before XPS measurements so that it is assumed that no traces of KPF_6 salt or solvents were left on the electrode surface. After rinsing, electrodes were transferred directly into the XPS machine from an argon-filled glove box connected to the XPS machine, ensuring that the samples never encountered air.

3. RESULTS AND DISCUSSION

3.1. OCV temperature impact

Fig. 1. compares the capacity retention of KVPFO//graphite full coin-cells after OCV for 12 h at different temperatures (20, 40 and 60°C). The cell with an OCV at 20°C underwent a faster capacity loss than the cells with OCV at 40°C and 60°C. Indeed, the three cells were similarly stable during the first 10 cycles while the capacity loss suddenly increased after 10 cycles for the cell with the OCV at 20°C. The reversible capacities obtained during the first cycle for the three cells suggest that the 12 h of OCV is enough to wet both graphite and KVPFO electrodes. Thus, the observed difference in capacity retention most likely originates from a pre-formation of an SEI spontaneously without cycling during the OCV. This is supported by the increase of the coulombic efficiency (CE) during the first cycle, from 46% to 62% then 67% as the OCV temperature increased from 20°C to 40°C then 60°C. Interestingly, the CE followed $CE_{40°C} > CE_{60°C} > CE_{20°C}$ after only few cycles and until the end of the cycling. These results thus highlight that high-temperature OCV minimizes the irreversible capacity in the first cycle due to the pre-formation of a SEI, which leads to better CE and capacity retention for prolonged cycling. Overall, the cell with an OCV at 40°C shows the best CE evolution and capacity retention compared to other cells. In contrast, an OCV at 60°C can be here considered too extreme to pre-form efficiently the SEI. Finally, after 50 cycles, the KVPFO//graphite cells with 12 h OCVs at 25, 40, and 60°C delivered 13, 48, and 41 mAh g^{-1} with a capacity retention of 23, 70, and 57%, respectively.

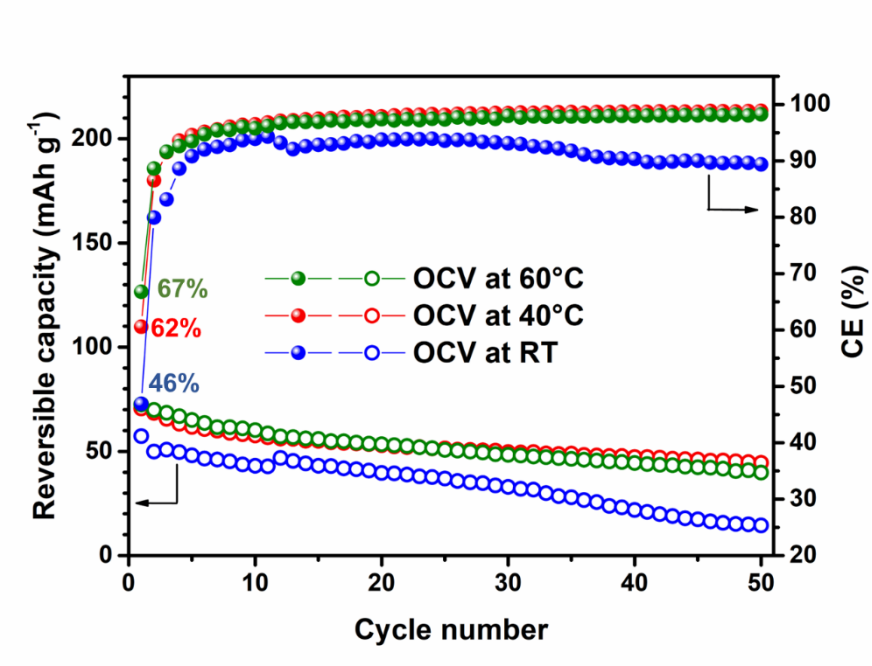

Fig. 1. Capacity retention and coulombic efficiency evolution obtained between 1.2 and 4.8 V at C/10 rate over 50 cycles for KVPFO//graphite coin-cells.

Then, XPS analysis was performed to confirm the pre-formation of a passivation layer and to evaluate the impact of the temperature on this phenomenon. **Fig. 2** shows the relevant XPS core level spectra (C 1s, K 2p, and O 1s) of fresh graphite and KVPFO electrodes, along with the electrodes as obtained from KVPFO//graphite cells after OCV at 25°C, 40°C, and 60°C. For clarity, **Fig. 2** also shows the main compounds (in at.%) as obtained from XPS quantification for the corresponding electrodes while the full XPS quantification can be found in **Table S1 and S2**.

First, regarding the peak attribution, the C 1s and K 2p of the graphite electrode (**Fig. 2. a and b**) display different peaks at 284.4, 285.0, 285.8 eV corresponding to C=C (carbon black and graphite), hydrocarbon contamination, carbon atoms in the C-O environment, respectively. The CMC and SBR binders display two characteristic peaks at 287 and 288.7 eV, assigned to CO- and CO_2-like carbon atoms, respectively [24]. At about 291.5 eV is a shake-up satellite (pi–pi* transitions of carbon black). The K 2p peaks at 293.5 (K $2p_{3/2}$) and 296.3 (K $2p_{1/2}$) eV are assigned to KF and ROK components. The other K 2p peaks at 294.8 and 297.4 eV are ascribed to K_xPF_y. Moreover, The O1s core peaks spectra show the presence of ROK and CO_2 environment at 531.8 eV. The peak displayed at 533.5 eV relates to CO based species [23].

For KVPFO (**Fig. 2. d and e**), C1s core peaks spectra exhibit different components at 284.5, 287, 288.7 eV attributed to C=C (carbon black) and carbon atoms in the CO and CO_2 environments, respectively. The PVDF binder shows two characteristic peaks at 286 and 290.5 eV, allocated to CH_2- and CF_2-like carbon atoms, respectively **[12]**. The K 2p peaks at 292.6 (K $2p_{1/2}$) and 295.4 (K $2p_{3/2}$) eV are assigned to KF, KVPFO, and ROK components [14]. The other K 2p peaks at 294.7 (K $2p_{1/2}$) and 297.5 (K $2p_{3/2}$) eV are ascribed to the K_xPF_y component . In addition, The O1s core peaks spectra show the presence of a KVPFO oxygen lattice (O^{2-}) at 530.7 eV [25]. The peak displayed at 532.2 eV is related CO and ROK, and the peak at 533.8 eV is assigned to a C-O environment [23]. Thus, quantification details for the graphite and KVPFO electrodes are given in **Tables S1 and S2** (supplementary information).

Regarding the electrodes surface composition, the comparative passivation layer evolution of fresh and assembled graphite and KVPFO electrodes by XPS at several OCV temperatures for 12h is displayed in **Fig. 2. a, b, d, and e**. The graphite and KVPFO passivation layers get thicker as a function of temperature without cycling with a remarkable increase in the CH, CO, KF, ROK, and K_xPF_y peak areas, indicating more salts and solvents decomposition at high OCV temperature (at 40 and 60°C). The 60°C OCV provides a large degradation of the solvents (**Fig. 2. c and f**), which is confirmed by the high initial coulombic efficiency of 67% and exhibited by the considerable increase in the CH, CO, and ROK peaks areas **(Fig. 2. a, b, d, and e, tables S1 and S2)** [5]. As shown in **Fig. 2. c and f** , the amounts of organic byproducts containing carbon and oxygen, as well as a smaller fraction of potassium, phosphorus, and fluorine inorganic species are more significant for graphite and KVPFO with a 60°C OCV. Thus, a more organic SEI appears unsuitable for the electrochemical performance (long-term cycling). Furthermore, **Fig. 2. c and f** show a 3D pie chart resulting from the SEI composition obtained from XPS quantification for fresh and assembled electrodes at different wetting temperatures. The passivation layer components have been divided into four parts: KPF_6 and its other by-products, organic species, KF, and binder. Indeed, increasing the OCV temperature involves more SEI growth; quantification of passivation layer for graphite electrodes with OCV temperatures of 25, 40, and 60°C could be respectively considered as 42.2, 58.8, and 66.9%. For KVPFO electrodes, the quantification of passivation layer could be respectively considered as 33.4, 52.3, and 50.8% with OCV temperatures of 25, 40, and 60°C. The high-temperature OCV can eliminate inhomogeneous reactions before cycling and minimize the irreversible capacity in the first cycle due to the

pre-formed passivation layer, which is consistent with the electrochemical results. For the rest of the study, the 12h OCV at 40°C was selected as an optimal parameter.

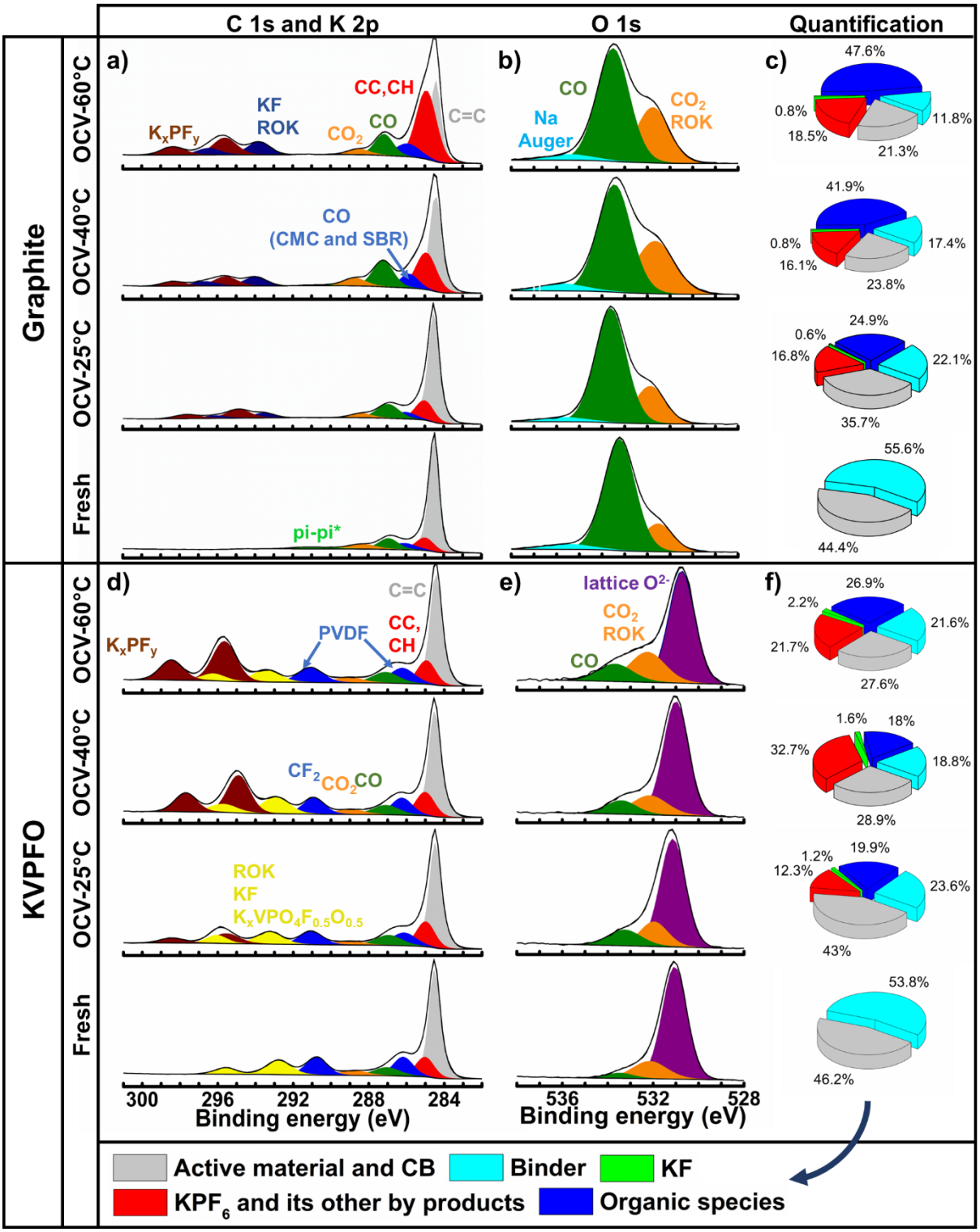

Fig. 2. a) C 1s, K 2p, **b)** O 1s XPS core level spectra, and **c)** Surface composition resulting from XPS quantification of graphite **d)** C 1s, K 2p, **e)** O 1s XPS core level spectra, and **f)** Surface composition resulting from XPS quantification of KVPFO electrodes as obtained

from KVPFO//graphite cells after OCV at different temperatures (25°C, 40°C, and 60°C) compared to the fresh graphite and KVPFO electrodes.

3.2. Upper cut-off voltage impact

The upper cut-off voltage (UCV) also affects the capacity retention. In this part, three full-cells were cycled at a C/10 rate to upper cut-off voltages of 4.5, 4.8, and 5 V over 50 cycles (**Fig. 3**). When the upper cut-off voltage of 4.5 V is applied, the reversible capacity decreases faster upon cycling compared to 4.8 and 5 V. This effect can be explained by the fact that total potassium intercalation into graphite occurs at potentials above 4.5 V, and the last KVPFO plateau was not reached. In addition, the larger capacity loss could also originate from a non-passivating and/or non-stable SEI formation at 4.5 V. When cycled above 4.5 V, the SEI is expected to be thicker, which may lead to better passivation. Indeed, increasing the upper cut-off voltage to 4.8 V leads to an initial CE of 62 % while a further increase to 5 V negatively impacts the first CE (53%). Moreover, after 30 cycles, the CE became almost stable at 99% and 96% corresponding to a capacity retention 70 % (48 mAh g^{-1}) and 63% (45 mAh g^{-1}) when cycled at 4.8 V and 5 V, respectively. Overall, the 4.8 V upper cut-off voltage can be considered as good compromise to limit the electrolyte reactivity (*i.e.* SEI formation) without decreasing to much the delivered capacity while the 5 V CU limit can be considered to extreme due to the much higher electrolyte degradation. The SEI formed at 5 V is thus more likely thicker but more unstable and/or non-passivating compared to the SEI formed at 4.8 V. Note that optimizing the KVPFO/graphite capacity ratio as function of the upper cut-off voltage would be necessary and would more likely help to further increase the CE and capacity retention, but this evaluation is out of the scope of this study.

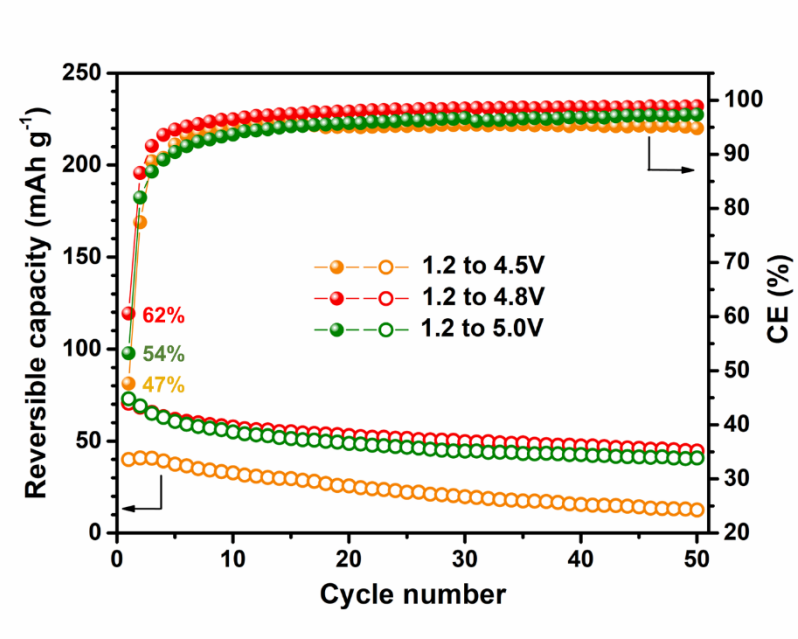

Fig. 3. Capacity retention and coulombic efficiency evolution obtained between 1.2-4.5 V, 1.2-4.8 V, and 1.2-5.0 V at C/10 rate over 50 cycles for KVPFO//graphite coin-cells.

Moreover, XPS analysis was used to observe the electrode/electrolyte interfaces by investigating the elemental compositions and the SEI growth built on the surfaces of the graphite and KVPFO electrodes and thus impacting their electrochemical performance. **Fig. 4** illustrates the combined regions of C 1s, K 2p and O 1s, V 2p core levels spectra of graphite and KVPFO at the three different UCVs after 50 cycles mentioned previously.

The C 1s and K 2p core spectra indicate that the passivation layer is thin on both electrodes at 4.5 UCV, as evidenced by the presence of characteristic peaks of the fresh materials. This result could be attributed to insufficient SEI growth and huge electrolyte consumption during 50 cycles, implying thus poor electrochemical performance [26].

The spectra and quantification tables for KVPFO show no significant differences between the UCVs of 4.8 and 5V (**Table S2, Fig. 4c and f**). However, in the case of the graphite electrode, increasing the UCVs results in a greater passivation layer. This layer exhibits organic composition at 4.5V due to the high degradation of EC and DEC solvents. Specifically, only 8.8% of KPF_6 and its by-products, as well as 46.2% of organic species. At 5V, both salt and solvent degradation is higher with 21.3% of KPF_6 and its by-products, and 47.7% of organic species.

Furthermore, the evolution of the atomic percentage of both electrodes detected by XPS at several UCVs is displayed in **Fig. 4. c and f**. It illustrates different behaviors concerning

passivation layer covering depending on the UCV chosen. Indeed, inner inorganic SEI to a certain amount should be preferred because compounds including K_2CO_3, KF, and other salt by-products improve SEI stability [27]. The passivation layer should present the best compromise between organic and inorganic compounds to ensure high SEI stability. Based on the electrochemical performance and XPS quantification (**Fig. 3 and 4**), UCV of 4.8 provide the best trade-off between organic and inorganic passivation layer (11.3% of K_2CO_3 and KF, 18.6% of KPF_6 and its other by-products, as well as 40.6% of organic species).

In addition to the chemical environment of the native material before cycling (**Fig. 2**), the O 1s and V 2p graphite core spectra show the presence of additional peaks (V $2p_{3/2}$ and V $2p_{1/2}$) at UCVs of 4.5, 4.8, and 5.0V. These peaks are related to vanadium dissolution resulting from the degradation of KVPFO and/or active material surface defects, which could explain partially the capacity losses over 50 cycles. This vanadium dissolution is more pronounced at a 5 V UCV (2.9%), as shown in **Fig. 4**. The 4.8 V UCV appears as an optimal cut-off voltage for the next part of the study.

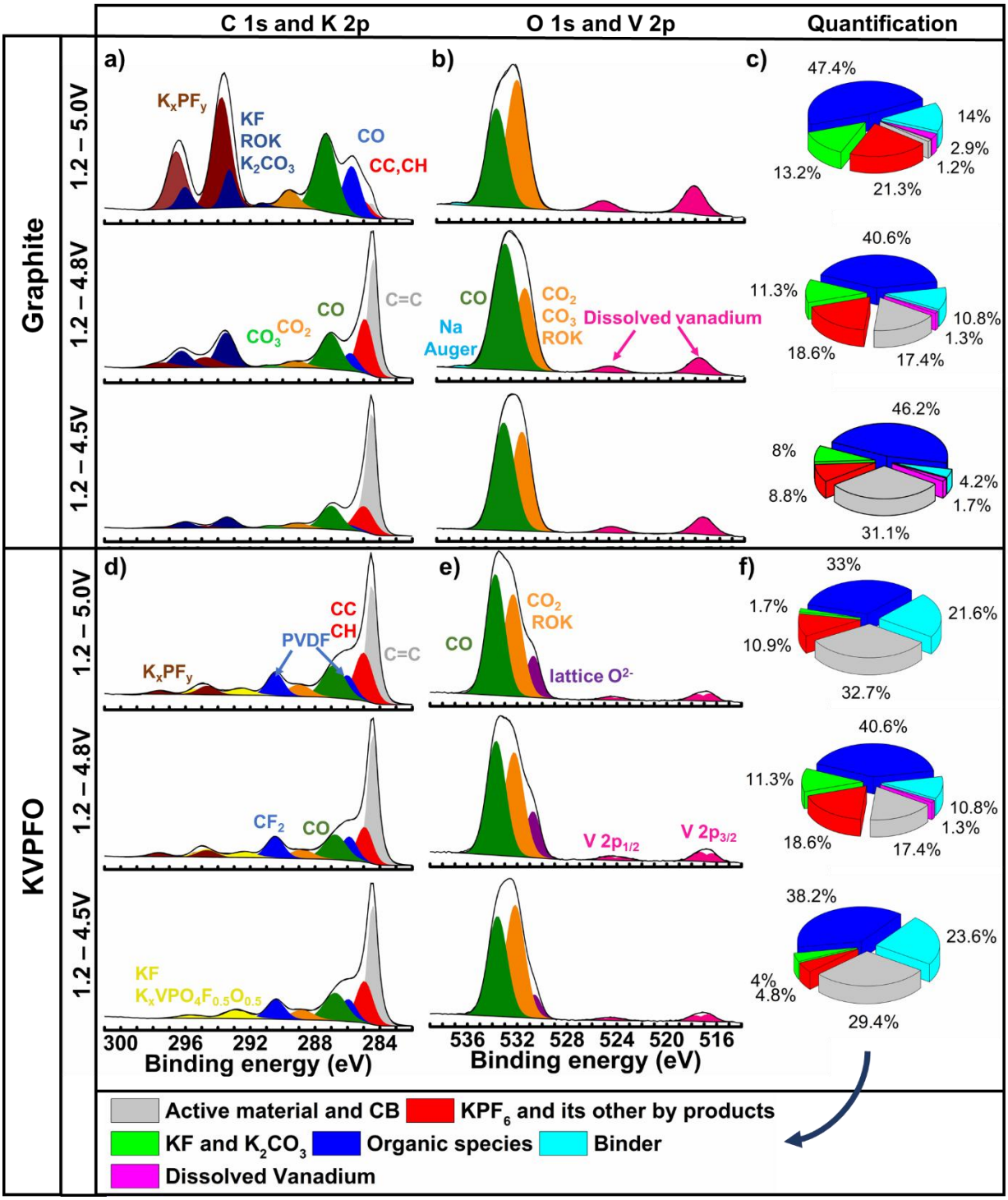

Fig. 4. a) C 1s, K 2p, **b)** O 1s XPS core level spectra, and **c)** Surface composition resulting from XPS quantification of graphite **d)** C 1s, K 2p, **e)** O 1s XPS core level spectra, and **f)** SEI composition resulting from XPS quantification of KVPFO electrodes as obtained from KVPFO//graphite cells after 50 cycles at different upper cut-off voltages (4.5, 4.8, and 5.0V).

3.3. Depth of discharge impact

The depth of discharge (DOD) has a significant impact on cell degradation due to both different SEI formation mechanisms (including SEI rearrangement/dissolution at higher DOD) and volume change of particles, which may result in electrolyte drying, stress, and cracking [27,28].

KVPFO//graphite full-cells were cycled with a selected upper cut-off voltage of 4.8 V and discharged to various DODs, *i.e.* to 1.2, 2.0, and 3.0 V (**Fig. 5**). A DOD of 3 V provided the largest loss of capacity and lowest CE upon cycling. Note that at 3V, the deintercalation of potassium ions from the graphite does not reach the final stage, which is consistent with the low CE that remains lower than 97% and a continuous SEI growth over cycles. In contrast, the 1.2 and 2.0 V DODs have similar electrochemical performance: a capacity retention of 70% with a capacity of 48 mAh g^{-1} and a CE of 99.3 % after 50 cycles. Overall, while higher DODs (*i.e.* lower discharge voltage) generally result in higher capacity fade and impedance growth, the opposite is observed here, which needs to be understood by the SEI analysis.

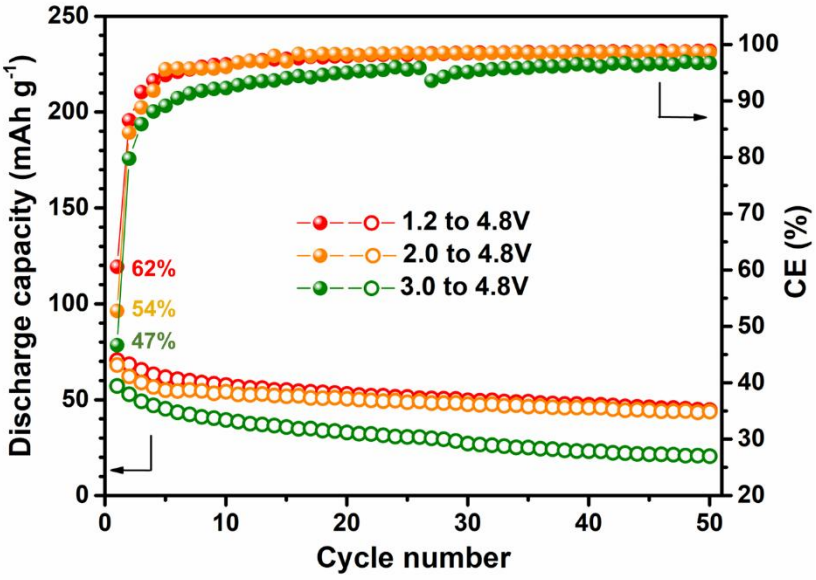

Fig. 5. Capacity retention and coulombic efficiency evolution obtained between 1.2-4.8 V, 2.0-4.8 V, and 3-5.0 V at C/10 rate over 50 cycles.

C 1s and K 2p core peaks spectra of the graphite electrode show that the passivation layer is thicker by increasing the discharge potential (from 1.2 to 3 V), As shown in **Fig. 6 a, b, d, and e**. This could be justified by the greater SEI dissolution/reorganization at higher DOD

(1.2 V). Moreover, the O 1s and V 2p graphite core spectra show the presence of additional peaks (V $2p_{3/2}$ and V $2p_{1/2}$). As noted, the vanadium dissolution related peaks resulting from the degradation of KVPFO or/and framework defects; this vanadium dissolution is more pronounced at a higher DOD of 1.2 V (1.3%), as shown in **Fig. 6**. On the other hand, KVPFO follows the same trend as graphite for 1.2 and 2V DODs except for 3V, where the SEI is much thinner (**Fig 6. c and f**). This may be a result of the excessive consumption of electrolytes upon the SEI growth on the anode, and the dissolution of the organic passivation layer on the cathode, since there will be no total deintercalation of potassium ions from the graphite at 3 V, thus fewer desolvation phenomena that reduce the thickness of the SEI. Finally, we can conclude that a thick SEI on the anode and a thin passivation layer on the cathode are observed. These results are consistent with CE evolution shown in **Fig. 5,** demonstrating the process (charge/discharge) irreversibility due to the inhomogeneous passivation layer growth at 3 V DOD. **Fig 6. c and f** show that the inorganic/organic species ratio of graphite electrodes provides 0.73, 1.1, and 0.4 for 1.2, 2.0, and 3.0 V, respectively. These results confirm that the more inorganic SEI is suitable for high electrochemical performance, as mentioned previously. Moreover, the passivation layer is more important in the case of graphite which suffers from several drawbacks; in particular, during potassiation the volume expansion (>60%) and the graphene layers exfoliation in the case of an unstable SEI, contrary to KVPFO, which has a three-dimensional framework that is more stable [19].

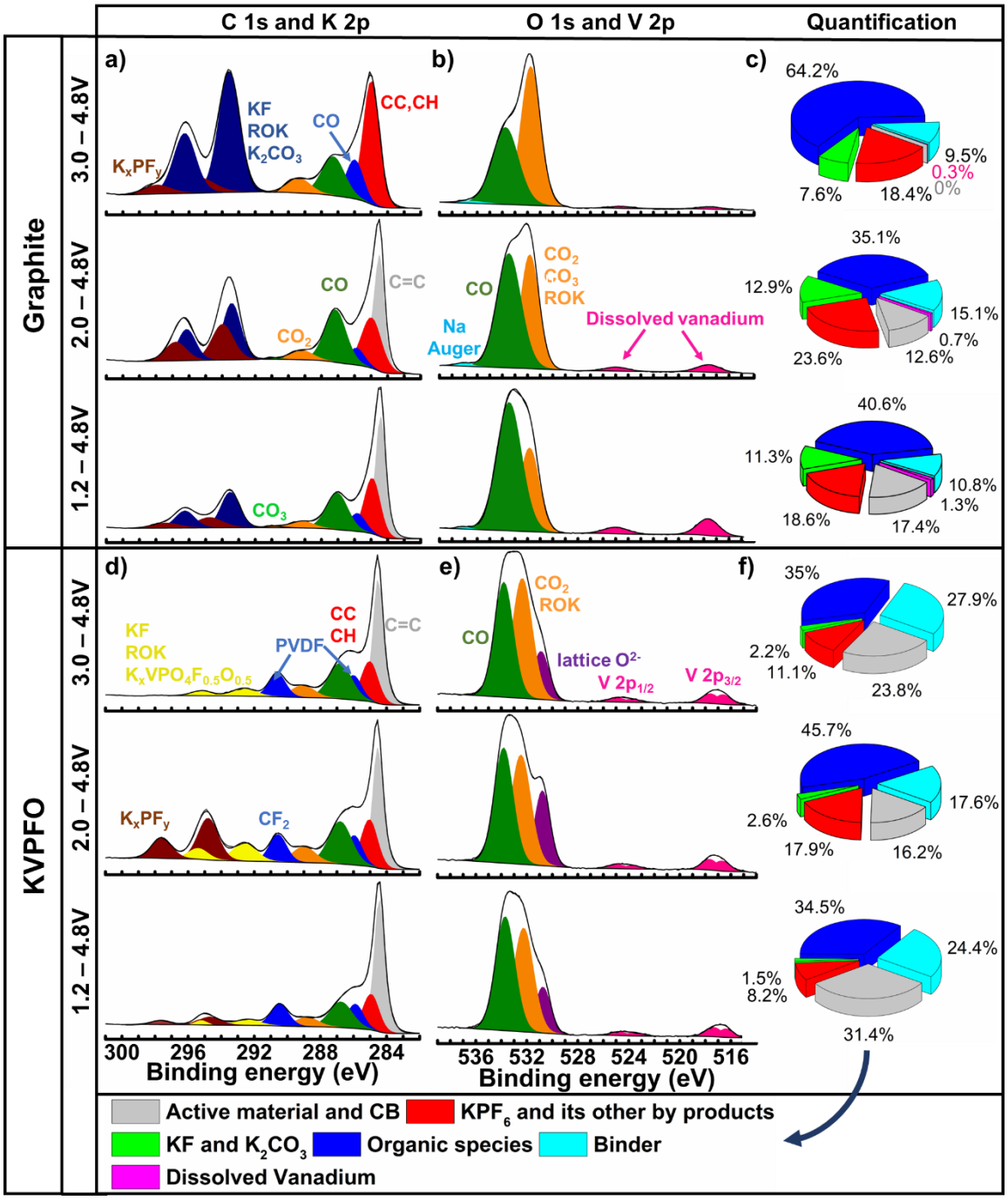

Fig. 6. a) C 1s, K 2p, **b)** O 1s XPS core level spectra, and **c)** Surface composition resulting from XPS quantification of graphite **d)** C 1s, K 2p, **e)** O 1s XPS core level spectra, and **f)** SEI composition resulting from XPS quantification of KVPFO electrodes as obtained from KVPFO//graphite cells after 50 cycles at different lower cut-off voltages (1.2, 2.0, and 3.0V).

As previously mentioned, a partial capacity loss comes from the dissolution of vanadium from the cathode, which is deposited on the anode surface and might contaminate the SEI of the

graphite. The mechanism of vanadium accumulation's detrimental effect on the graphite electrode in KIBs is poorly studied in the literature compared to transition metal dissolutions in Li-ion batteries, especially in the spinel structure-type [29,30]. Indeed, the oxidation state of vanadium species on the graphite electrode is critical for thoroughly understanding these processes. The vanadium oxidation state present in the pristine KVPFO material is V^{3+}. Fig. **S1. b** shows a shift to high binding energy at the V $2p_{3/2}$ peaks after the first cycle (i.e., a degree of oxidation slightly higher than 3^{+}) on the graphite electrode, which indicates that oxidized vanadium dissolution takes place at high potential and before to be reduced on the graphite negative electrode. As depicted in **Fig. S1 a and b**, in an actual battery cell, the consequence could be ongoing active potassium loss and increased SEI growth, exhibited by the continual CE increase. Accordingly, this vanadium dissolution starting from the first cycle might be the underlying mechanism causing the enhanced capacity fading observed for graphite/KVPFO full cell when operating under conditions favoring vanadium dissolution (i.e., high upper cut-off voltages).

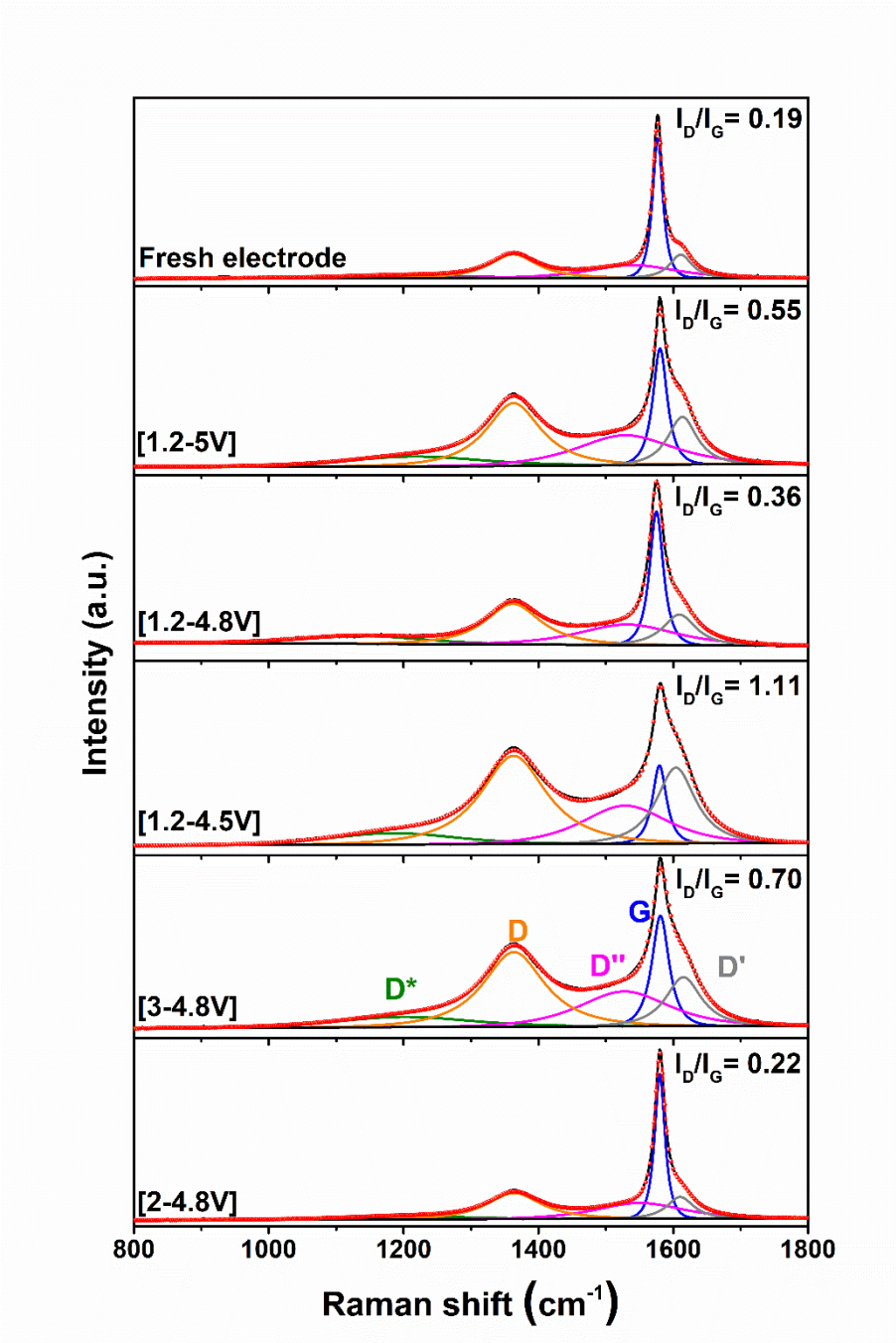

Fig. 7. Raman spectra of graphite electrodes from full-cells after 50 Cycles at different potential windows.

To examine the structural stability of graphite under various potentials after 50 cycles, XRD was conducted as part of further investigation (Fig. S3). For KVPFO, It was previously demonstrated by Wernert et al, [19] that the material exhibited a stable structure even after undergoing up to 5V. Furthermore, the **Fig. S3** shows the main characteristic Bragg peak (002) of graphite at 22°. After cycling a shoulder in the graphite peak (002) is systematically observed whatever the potential windows used [31]. This peak shoulder highlights the

presence of potassium ions inserted within the electrode structure, as also shown from the peaks labeled KC_{36} at xx° and KC_{24} at xx° which are intermediate potassiated phases. The presence these peaks and the absence of KC_8 characteristic peak (16.6°) are in line with a limited potassiation [32]. For further investigations, Raman spectroscopy analysis was carried out on the same set of electrodes.

Fig. 7 shows two characteristic bands of defective or disordered carbon around 1360 cm^{-1} (D-band) and graphitized sp^2 carbon around 1580 cm^{-1} (G-band). These peaks were fitted with a Lorentzian shaped-bands to determine the I_D/I_G ratio with precision, where I_D and I_G are the intensities of the fitted D-peak and G-peak, respectively [33–35].

The rise in the ratio of D-band and G-band intensities (I_D/I_G) observed in the Raman spectrum of a graphite electrode is usually attributed to three factors: the trapped K ions into the graphite structure, intercalation process, and the structure exfoliation, indicating a decrease in the graphite crystallinity, which could be one of the key factors behind the capacity decay [36].

On the one hand, with an UCV of 4.5V (1.2-4.5V) and a DOD of 3V (3-4.8V) after 50 cycles the spectra presents the highest I_D/I_G of 1.11 and 0.70, respectively, which is due to the trapping of K ions into the graphite structure upon cycling, agreeing with the electrochemical results (**Fig. 3 and 5**). On the other hand, cells cycled at potential windows of [1.2-5V], [1.2-4.8V], and [2-4.8V] exhibit lower I_D/I_G of 0.55, 0.36, and 0.22 respectively. Thus, the Raman spectra after 50 cycles at voltage window of [2-4.8V], showing a close I_D/I_G ratio to that of fresh electrode, indicates that the structure of graphite is intact after repeated K-ion intercalation/deintercalation, which is consistent with the previously discussed electrochemical performance and SEI characterization.

3.4. Power performance

In this part, a rate capability test was performed using the 4.8 V upper cut off-voltage and the 1.2 and 2 V DODs as they were similar in term of capacity retention. Note that high rate at low discharge voltage may result in K plating, higher polarization, and cell degradation [20,37]. As expected, **Fig. 8** shows that using 2 V as DOD led to higher capacity at high rate (~50 mAh g^{-1} at 2C with a polarization of 0.8 V), which is quite satisfying for such relatively

high KVPFO/graphite loading ratio (2/5 mg cm^{-2}). In contrast, the 1.2 V DOD led to only ~35 mAh g^{-1} at C/2 with a higher polarization of 1.1 V, indicating an impedance growth due to a different SEI formation. Overall, these results highlight that KVPFO//graphite full-cells with relatively high energy (42 Wh kg_{device}^{-1} at C/5 and 31.5 Wh kg_{device}^{-1} at 2C) and high power (8.4 W kg_{device}^{-1} at C/5 and 63 W kg_{device}^{-1} at C/5) can be obtained. Note that the energy and power values given here include the active materials, binder, carbon additive, electrolyte, and current collector masses. Moreover, further improvement is expected, especially as the KVPFO electrode and the electrolyte formulation still need to be optimized (addition of additives).

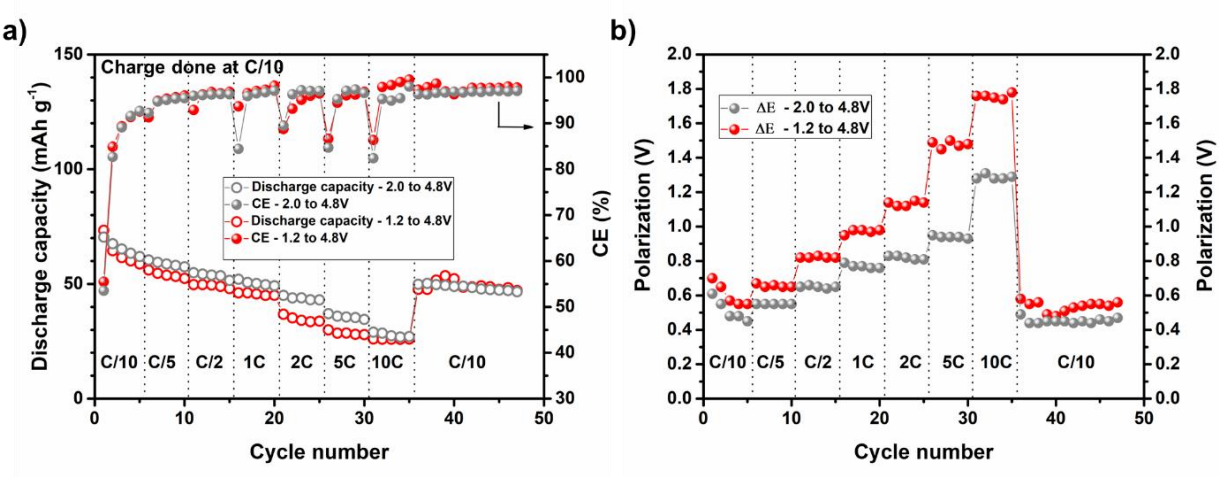

Fig. 8. a) Galvanostatic rate performance at 1.2V and 2.0V DODs from C/10 to 10C and **b)** corresponding polarization of graphite/KVPFO full coin cells.

4. CONCLUSIONS

This work studied the impact of OCV temperature, UCVs, DODs and rates of cycling of KVPFO/graphite full cells on the electrochemical performance through SEI studies. After cycling, cells underwent XPS analysis to study the mentioned parameters on the passivation layer. The main results of this work can be summarized as follows:

- Passivation layer preformation on KVPFO and graphite is more pronounced by increasing the OCV temperature, likely to rise the electrode wetting by electrolyte. A OCV temperature at 40°C for 12h leads to a main inorganic behavior, and consequently to good electrochemical performance compared to 25 and 60°C.
- The passivation layer is nearly absent on both cathode and anode electrodes at 4.5 UCV, leading to critical electrochemical results. In contrast, UCV of 4.8 provided the

best trade-off between the organic and inorganic passivation layer, leading to both good capacity retention and coulombic efficiency evolution, compared to 4.5 and 5 V UCVs.

- Greater SEI dissolution at 1.2V compared to 2V DODs lead to a thinner SEI. Furthermore, the ratio of SEI inorganic/organic species for graphite electrodes are 0.73, 1.1, and 0.4 for 1.2, 2.0, and 3.0 V. Suitable electrochemical performance is observed when this ratio is close to 1 corresponding likely to a stable passivation layer.
- For graphite/KVPFO full cell, capacity loss comes partially from vanadium dissolution that started from the 1st cycle.
- 1.2V DOD presented lower capacity at a high rate, indicating an impedance growth at higher DODs, confirmed by the increase of polarization as a function of current density. In contrast, 2 V DOD led to higher capacity at a high rate.

This work highlights the correlation between SEI investigation and electrochemical performance. This study could be completed in the future by the coating and optimization of KVPFO electrode, as well as the formulation of new innovative electrolytes to mitigate the vanadium dissolution and improve the passivation layer stability.

REFERENCES

[1] B. Diouf, R. Pode, Potential of lithium-ion batteries in renewable energy, Renew. Energy. 76 (2015) 375–380. https://doi.org/10.1016/j.renene.2014.11.058.

[2] S. Dhir, S. Wheeler, I. Capone, M. Pasta, Outlook on K-Ion Batteries, Chem. 6 (2020) 2442–2460. https://doi.org/10.1016/j.chempr.2020.08.012.

[3] T. Hosaka, K. Kubota, A.S. Hameed, S. Komaba, Research Development on K-Ion Batteries, Chem. Rev. 120 (2020) 6358–6466. https://doi.org/10.1021/acs.chemrev.9b00463.

[4] T. Hosaka, K. Kubota, A.S. Hameed, S. Komaba, Research Development on K-Ion Batteries, Chem. Rev. 120 (2020) 6358–6466. https://doi.org/10.1021/acs.chemrev.9b00463.

[5] H. Wang, D. Zhai, F. Kang, Solid electrolyte interphase (SEI) in potassium ion batteries, Energy Environ. Sci. 13 (2020) 4583–4608. https://doi.org/10.1039/D0EE01638A.

[6] L. Madec, V. Gabaudan, G. Gachot, L. Stievano, L. Monconduit, H. Martinez, Paving the Way for K-Ion Batteries: Role of Electrolyte Reactivity through the Example of Sb-Based Electrodes, ACS Appl. Mater. Interfaces. 10 (2018) 34116–34122. https://doi.org/10.1021/acsami.8b08902.

[7] H. Onuma, K. Kubota, S. Muratsubaki, T. Hosaka, R. Tatara, T. Yamamoto, K. Matsumoto, T. Nohira, R. Hagiwara, H. Oji, S. Yasuno, S. Komaba, Application of Ionic

Liquid as K-Ion Electrolyte of Graphite//K2Mn[Fe(CN)6] Cell, ACS Energy Lett. (2020) 2849–2857. https://doi.org/10.1021/acsenergylett.0c01393.

[8] Z. Wu, J. Zou, S. Shabanian, K. Golovin, J. Liu, The roles of electrolyte chemistry in hard carbon anode for potassium-ion batteries, Chem. Eng. J. 427 (2022) 130972. https://doi.org/10.1016/j.cej.2021.130972.

[9] L. Caracciolo, L. Madec, G. Gachot, H. Martinez, Impact of the Salt Anion on K Metal Reactivity in EC/DEC Studied Using GC and XPS Analysis, ACS Appl. Mater. Interfaces. 13 (2021) 57505–57513. https://doi.org/10.1021/acsami.1c19537.

[10] S. Su, Q. Liu, J. Wang, L. Fan, R. Ma, S. Chen, X. Han, B. Lu, Control of SEI Formation for Stable Potassium-Ion Battery Anodes by Bi-MOF-Derived Nanocomposites, ACS Appl. Mater. Interfaces. 11 (2019) 22474–22480. https://doi.org/10.1021/acsami.9b06379.

[11] Z. T. Gossage, T. Hosaka, T. Matsuyama, R. Tatara, S. Komaba, Fluorosulfonamide-type electrolyte additives for long-life K-ion batteries, J. Mater. Chem. A. 11 (2023) 914–925. https://doi.org/10.1039/D2TA06926A.

[12] A.J. Naylor, M. Carboni, M. Valvo, R. Younesi, Interfacial Reaction Mechanisms on Graphite Anodes for K-Ion Batteries, ACS Appl. Mater. Interfaces. 11 (2019) 45636–45645. https://doi.org/10.1021/acsami.9b15453.

[13] C. Liu, S. Luo, H. Huang, Y. Zhai, Z. Wang, Layered potassium-deficient P2- and P3-type cathode materials KxMnO2 for K-ion batteries, Chem. Eng. J. 356 (2019) 53–59. https://doi.org/10.1016/j.cej.2018.09.012.

[14] T. Hosaka, T. Matsuyama, K. Kubota, S. Yasuno, S. Komaba, Development of KPF_6 /KFSA Binary-Salt Solutions for Long-Life and High-Voltage K-Ion Batteries, ACS Appl. Mater. Interfaces. 12 (2020) 34873–34881. https://doi.org/10.1021/acsami.0c08002.

[15] L. Deng, Y. Zhang, R. Wang, M. Feng, X. Niu, L. Tan, Y. Zhu, Influence of KPF6 and KFSI on the Performance of Anode Materials for Potassium-Ion Batteries: A Case Study of MoS2, ACS Appl. Mater. Interfaces. 11 (2019) 22449–22456. https://doi.org/10.1021/acsami.9b06156.

[16] J.-Y. Hwang, J. Kim, T.-Y. Yu, H.-G. Jung, J. Kim, K.-H. Kim, Y.-K. Sun, A new P2-type layered oxide cathode with superior full-cell performances for K-ion batteries, J. Mater. Chem. A. 7 (2019) 21362–21370. https://doi.org/10.1039/C9TA07837A.

[17] F. Allgayer, J. Maibach, F. Jeschull, Comparing the Solid Electrolyte Interphases on Graphite Electrodes in K and Li Half Cells, ACS Appl. Energy Mater. 5 (2022) 1136–1148. https://doi.org/10.1021/acsaem.1c03491.

[18] Z. Liu, J. Wang, B. Lu, Plum pudding model inspired KVPO4F@3DC as high-voltage and hyperstable cathode for potassium ion batteries, Sci. Bull. 65 (2020) 1242–1251. https://doi.org/10.1016/j.scib.2020.04.010.

[19] R. Wernert, L.H.B. Nguyen, E. Petit, P.S. Camacho, A. Iadecola, A. Longo, F. Fauth, L. Stievano, L. Monconduit, D. Carlier, L. Croguennec, Controlling the Cathodic Potential of $KVPO_4F$ through Oxygen Substitution, Chem. Mater. 34 (2022) 4523–4535. https://doi.org/10.1021/acs.chemmater.2c00295.

[20] B. Larhrib, L. Madec, L. Monconduit, H. Martinez, Optimized electrode formulation for enhanced performance of graphite in K-ion batteries, Electrochimica Acta. 425 (2022) 140747. https://doi.org/10.1016/j.electacta.2022.140747.
[21] B. Larhrib, L. Madec, Toward highly reliable K-ion half and full coin cells, Batter. Supercaps. n/a (n.d.) e202300061. https://doi.org/10.1002/batt.202300061.
[22] L. Caracciolo, L. Madec, E. Petit, V. Gabaudan, D. Carlier, L. Croguennec, H. Martinez, Electrochemical Redox Processes Involved in Carbon-Coated KVPO4F for High Voltage K-Ion Batteries Revealed by XPS Analysis, J. Electrochem. Soc. 167 (2020) 130527. https://doi.org/10.1149/1945-7111/abbb0c.
[23] L. Caracciolo, L. Madec, H. Martinez, XPS Analysis of K-based Reference Compounds to Allow Reliable Studies of Solid Electrolyte Interphase in K-ion Batteries, ACS Appl. Energy Mater. 4 (2021) 11693–11699. https://doi.org/10.1021/acsaem.1c02400.
[24] A. Darwiche, L. Bodenes, L. Madec, L. Monconduit, H. Martinez, Impact of the salts and solvents on the SEI formation in Sb/Na batteries: An XPS analysis, Electrochimica Acta. 207 (2016) 284–292. https://doi.org/10.1016/j.electacta.2016.03.089.
[25] Y.-C. Lu, E.J. Crumlin, G.M. Veith, J.R. Harding, E. Mutoro, L. Baggetto, N.J. Dudney, Z. Liu, Y. Shao-Horn, In Situ Ambient Pressure X-ray Photoelectron Spectroscopy Studies of Lithium-Oxygen Redox Reactions, Sci. Rep. 2 (2012) 715. https://doi.org/10.1038/srep00715.
[26] F. German, A. Hintennach, A. LaCroix, D. Thiemig, S. Oswald, F. Scheiba, M.J. Hoffmann, H. Ehrenberg, Influence of temperature and upper cut-off voltage on the formation of lithium-ion cells, J. Power Sources. 264 (2014) 100–107. https://doi.org/10.1016/j.jpowsour.2014.04.071.
[27] R. Gauthier, A. Luscombe, T. Bond, M. Bauer, M. Johnson, J. Harlow, A. Louli, J.R. Dahn, How do Depth of Discharge, C-rate and Calendar Age Affect Capacity Retention, Impedance Growth, the Electrodes, and the Electrolyte in Li-Ion Cells?, J. Electrochem. Soc. (2022). https://doi.org/10.1149/1945-7111/ac4b82.
[28] A. Eldesoky, M. Bauer, T. Bond, N. Kowalski, J. Corsten, D. Rathore, R. Dressler, J.R. Dahn, Long-Term Study on the Impact of Depth of Discharge, C-Rate, Voltage, and Temperature on the Lifetime of Single-Crystal NMC811/Artificial Graphite Pouch Cells, J. Electrochem. Soc. 169 (2022) 100531. https://doi.org/10.1149/1945-7111/ac99a6.
[29] J. Wandt, A. Freiberg, R. Thomas, Y. Gorlin, A. Siebel, R. Jung, H.A. Gasteiger, M. Tromp, Transition metal dissolution and deposition in Li-ion batteries investigated by operando X-ray absorption spectroscopy, J. Mater. Chem. A. 4 (2016) 18300–18305. https://doi.org/10.1039/C6TA08865A.
[30] K. Kalaga, F.N. Sayed, M.-T.F. Rodrigues, G. Babu, H. Gullapalli, P.M. Ajayan, Doping stabilized Li3V2(PO4)3 cathode for high voltage, temperature enduring Li-ion batteries, J. Power Sources. 390 (2018) 100–107. https://doi.org/10.1016/j.jpowsour.2018.04.048.
[31] Z. Jian, W. Luo, X. Ji, Carbon Electrodes for K-Ion Batteries, J. Am. Chem. Soc. 137 (2015) 11566–11569. https://doi.org/10.1021/jacs.5b06809.
[32] X. Li, J. Li, L. Ma, C. Yu, Z. Ji, L. Pan, W. Mai, Graphite Anode for Potassium Ion batteries: Current Status and Perspective, ENERGY Environ. Mater. (2021) eem2.12194. https://doi.org/10.1002/eem2.12194.

[33] A. Sadezky, H. Muckenhuber, H. Grothe, R. Niessner, U. Pöschl, Raman microspectroscopy of soot and related carbonaceous materials: Spectral analysis and structural information, Carbon. 43 (2005) 1731–1742. https://doi.org/10.1016/j.carbon.2005.02.018.

[34] S. Yarova, D. Jones, F. Jaouen, S. Cavaliere, Strategies to Hierarchical Porosity in Carbon Nanofiber Webs for Electrochemical Applications, Surfaces. 2 (2019) 159–176. https://doi.org/10.3390/surfaces2010013.

[35] A.Y. Lee, K. Yang, N.D. Anh, C. Park, S.M. Lee, T.G. Lee, M.S. Jeong, Raman study of D* band in graphene oxide and its correlation with reduction, Appl. Surf. Sci. 536 (2021) 147990. https://doi.org/10.1016/j.apsusc.2020.147990.

[36] D. Wang, X. Du, B. Zhang, Solvent Molecular Design to Regulate the Intercalation Behavior in Ether Electrolyte for Stable Graphite Anodes in Potassium-Ion Batteries, Small Struct. 3 (2022) 2200078. https://doi.org/10.1002/sstr.202200078.

[37] K. Kubota, M. Dahbi, T. Hosaka, S. Kumakura, S. Komaba, Towards K-Ion and Na-Ion Batteries as "Beyond Li-Ion," Chem. Rec. 18 (2018) 459–479. https://doi.org/10.1002/tcr.201700057.